Modulational instability of multiple-charged optical vortex solitons under saturation of the nonlinearity

A. Dreischuh,[1,*] G. G. Paulus,[1] F. Zacher,[1] F. Grasbon,[1] D. Neshev,[2] and H. Walther[1]
[1]*Max-Planck-Institut für Quantenoptik, Hans-Kopfermann-Straße 1, 85748 Garching, Germany*
[2]*Department of Quantum Electronics, Sofia University, 5, J. Bourchier Blvd., 1164 Sofia, Bulgaria*
(Received 4 December 1998; revised manuscript received 28 July 1999)

We present a linear analysis and numerical simulations of the instability of optical vortex solitons (OVSs) of arbitrary topological charge. They show a rich variety of instability scenarios depending on the type of perturbation. The saturation of the nonlinearity is shown to be able to slow down the decay of multiple charged dark beams at an intermediate evolution stage and to prevent their ultimate decay into charge-1 OVSs. This concept is experimentally verified by the observation of a partial decay of a triple-charged OV beam and by comparing this dynamic with the behavior of OV beams of topological charges $m=1$, 2, 3, and 4. [S1063-651X(99)09912-2]

PACS number(s): 42.65.Tg, 42.65.Sf

I. INTRODUCTION

Recently, much attention in nonlinear optics has been attracted by the dark spatial solitons (DSSs) and, in particular, by the optical vortex solitons (OVSs) [1–3]. At the phase-singularity point arising from a screw-type phase distribution, the real and the imaginary parts of the field amplitude are zero (i.e., also the field intensity). As a result of the compensation of diffraction and nonlinearity in a self-defocusing nonlinear medium, the odd dark beam forms an OVS. From a mathematical point of view the screw-type phase profile is described by an $\exp(im\varphi)$ multiplier, where φ is the azimuthal coordinate. The integer number m is defined as the topological charge (TC), whereas its sign is determined by the direction of the dislocation.

Optical vortices appear in speckle fields [4], as modes in ring resonators with beam rotators [5], and can be born when a beam with a smooth wavefront passes through a Gaussian-like lens [6]. Optical vortices can also be produced by computer-generated holograms (CGHs) [7,8], by spiral phase plates [9], and by specially configured blazed gratings [10] in the submicrometer and millimeter wavelength region. Several effects have been discovered in recent years that promise interesting applications for OVSs: An optical transistor effect was found in the guiding efficiency of the gradient waveguide induced by an OVS [11]. The sum-frequency generation of light beams with screw-type phase dislocations offers the possibility to create vortices of different TCs [12] and provides new opportunities to construct an optical processor. Regardless of the potential applications, the generation of metastable OVSs of TCs $|m|\geqslant 1$ and the investigation of their modulational sensitivity is of increasing importance.

OVSs were first generated by using discrete ''spiral''-type phase masks [13] and by modulational instability of one-dimensional (1D) dark beams [14]. However, the use of CGHs [7] is more precise and practical [15]. In the case of an m-fold charged screw dislocation, the addition of a small coherent pedestal at the reproduction of the CGH gives rise to its splitting in m dislocations of charge 1 [16]. A theoretical and experimental study on the propagation and decay of highly charged optical vortices in a medium with an anisotropic nonlocal nonlinearity can be found in [17]. Even for an isotropic nonlinearity, the vortex dynamics of the nonlinear wave equation shows that OV beams of charge $|m|\geqslant 2$ are topologically unstable [18]. The suppression of the transverse instability by saturating the nonlinearity [3] allowed us recently to generate stable OVSs with TCs up to $m=4$ [19]. In order to identify clearly their formation, stability and decay are undoubtfully distinguished. This has led to the intriguing observation of a partial decay of threefold charged OVS into double- and single-charged OVSs. The latter motivated us to perform the present instability analysis.

II. THEORETICAL MODEL

The propagation of $(2+1)$-dimensional cw optical beams in a nonlinear medium is described by the generalized nonlinear Schrödinger equation (GNLSE) [20],

$$-i2k_0n_0\frac{\partial E}{\partial z}+\left(\frac{\partial^2}{\partial x^2}+\frac{\partial^2}{\partial y^2}\right)E+k_0^2f(|E|^2)E=0, \quad (2.1)$$

where k_0 is the vacuum wave number and n_0 is the linear refractive index of the medium. $E(x,y,z)$ is the slowly varying complex electric field amplitude, and $f(|E|^2)$ describes in a general form the nonlinear contribution to the refractive index

$$n^2(x,y,|E|^2)=n_0^2(x,y)+f(|E|^2). \quad (2.2)$$

In particular [1,21],

$$f(|E|^2)=\begin{cases}\alpha_1|E|^2,\\ n_0n_2|E|^2/(1+\gamma^2|E|^2n_2/n_0),\\ \alpha_1|E|^2-\alpha_2|E|^4,\end{cases} \quad (2.3)$$

*Permanent address: Sofia University, Department of Quantum Electronics 5, J. Bourchier Blvd., 1164 Sofia, Bulgaria. FAX: +3592/9625276. Electronic address: ald@phys.uni-sofia.bg

for Kerr-law, two-level saturable, and competing cubic-quintic nonlinearity ($\alpha_1\alpha_2<0$), respectively. With the substitution $g(|E|^2)=(-k_0/[2n_0])f(|E|^2)$, Eq. (2.1) can be rewritten in cylindrical coordinates which are natural for analyzing the evolution of OVSs. Accounting explicitly for the topological charge m of the OV beam,

$$E(r,z)=U(r,z)\exp(im\varphi), \tag{2.4}$$

the GNLSE is of the form [22]

$$i\frac{\partial U}{\partial z}+\beta\left(\frac{1}{r}\frac{\partial}{\partial r}+\frac{\partial^2}{\partial r^2}\right)U-\frac{\beta m^2}{r^2}U+g(|U|^2)U=0 \tag{2.5}$$

with $\beta=-k_0/(2n_0)$ being a negative constant. The 2D linear stability analysis presented in this section is similar to the $(1+1)$-dimensional model of Kivshar and co-workers [23]. Equation (2.5) has an exact solution of the form $U(r,z)=U_0(r,z)e^{[i(\omega r-kz)]}$, provided

$$k=\beta\omega^2-g(U_0^2)+\frac{\beta m^2}{r^2}. \tag{2.6}$$

The last term in Eq. (2.6) introduces a TC-dependent correction to the wave number. It is shown [20] that the transverse (azimuthal) phase gradient $\mathbf{k}_\perp$ along with the intensity gradient $\nabla_\perp(|\mathbf{E}|^2)$ rules the OV propagation dynamics. The optical equivalent of the fluid paradigm says [20] that the vortex trajectory (and stability) is affected by all other sources of $\mathbf{k}_\perp$ and $\nabla_\perp(|\mathbf{E}|^2)$ but not by itself. Because of the discontinuity of the phase distribution at the OV beam axis, the infinitely large values of k do not have a physical meaning. This agrees with the interpretation in [20] that at the center of the vortex core $\mathbf{k}_\perp$ should be viewed as a local average value of $\mathbf{k}_\perp$ in the vicinity of the core.

Further we look at a small-amplitude solution of the GNLSE in the form

$$U(r,z)=[U_0(r,z)+a(r,z)]e^{\{i[\omega r-k(r,z)z+\Phi(r,z)]\}}, \tag{2.7}$$

where $a^2\ll U_0^2$ and $\Phi(r,z)$ are the unknown perturbation amplitude and phase, respectively. Substituting Eq. (2.7) in Eq. (2.5), accounting for Eqs. (2.6), and keeping the linear terms of the perturbation amplitude a, we obtain the following system of equations:

$$a_z+2\beta(\omega+\Phi_r)a_r+(U_0+a)\left[\frac{\beta}{r}(\omega+\Phi_r)+\beta\Phi_{rr}\right]=0, \tag{2.8}$$

$$-\Phi_z(U_0+a)+\beta\left[a_{rr}+\left(\frac{a_r}{r}+\frac{m^2}{r^2}\right)\right.$$

$$\left.-(U_0+a)+(2\omega\Phi_r+\Phi_r^2)\right]+2U_0^2ag'(U_0^2)=0.$$

Within this linear instability analysis, nontrivial solutions

$$a=a_0\exp[i(\Omega r-\Theta z)], \tag{2.9}$$

$$\Phi=\Phi_0\exp[i(\Omega r-\Theta z)],$$

of Eq. (2.8) exist when the transverse spatial frequency Ω and the longitudinal wave number Θ of the perturbation simultaneously satisfy the conditions

$$(\Theta-2\Omega\omega\beta)^2+\beta\Omega^2[2U_0^2g'(U_0^2)-\beta\Omega^2]+\frac{\beta\Omega^2}{r}=0,$$

$$(\Theta-2\Omega\omega\beta)\frac{\beta\omega}{r}+\Omega[2U_0^2g'(U_0^2)-\beta\Omega^2]+\frac{\beta^2\Omega^3}{r}=0. \tag{2.10}$$

The result given by Eq. (2.10) refers to the $(2+1)$-dimensional case of nonlinear cw beam propagation. It generalizes the known results for the 1D GNLSE [23] and for the 1D NLSE (see, e.g., [1,2]). A formal transition to one transverse dimension can be done by neglecting the terms containing $(1/r)\partial/\partial r$ and $1/r^2$ in Eq. (2.5) and by interpreting r as the single transverse coordinate. In this case the conditions given by Eq. (2.10) become simpler and the critical transverse spatial frequency of the perturbation $\Omega_{\rm crit}$ is

$$\Omega_{\rm crit}^2=\frac{2U_0^2}{\beta}g'(U_0^2). \tag{2.11}$$

An instability region appears at $\beta g'(U_0^2)>0$ [i.e., at $f'(U_0^2)<0$]. For $\Omega<\Omega_{\rm crit}$, the initially small perturbation amplitude $a(r,z)$ grows exponentially and a modulational instability develops. In other words, the modulational sensitivity grows with the critical spatial frequency $\Omega_{\rm crit}$. Returning to the 2D case of interest in this work, we obtain

$$\Omega_{\rm crit}^2=\frac{[1/r+2U_0^2g'(U_0^2)][\omega^2+m^2/r^2]}{k+g(U_0^2)}$$

$$=\frac{[1/r-(k_0/n_0)U_0^2f'(U_0^2)][\omega^2+m^2/r^2]}{(k_0/2n_0)[1-f(U_0^2)]}. \tag{2.12}$$

It should be noted that $\Omega_{\rm crit}$ remains inverse proportional to the radial offset from the OV beam axis. Within the vortex core (and especially in the vicinity of the phase singularity, i.e., at $r\to0$) there are no rays with infinite wave numbers [20,24]. Therefore, $\Omega_{\rm crit}$ must remain a quantity of finite values within the core. For the second and third saturation model given in Eq. (2.3), $|f'(U_0^2)|$ and $\Omega_{\rm crit}$ are decreasing functions of the intensity. This confirms the general conclusion [1,3] that the saturation of the third-order nonlinearity is able to suppress effectively the modulational instability.

From Eq. (2.12) it is obvious that the increase of the TC m leads to higher values for the critical transverse spatial frequency of the perturbation $\Omega_{\rm crit}$ and, therefore, to an enhanced modulational sensitivity. In order to provide a framework to interpret an intriguing experimental observation (see [19] and Sec. II) we will formulate the following problem: Under which conditions (if any) can a charge-m OVS decay into a single- and an $(m-1)$-fold charged OVS. This does makes sense, of course, for $m=3$ or more. Intuitively, a perturbation with a transverse spatial frequency Ω satisfying

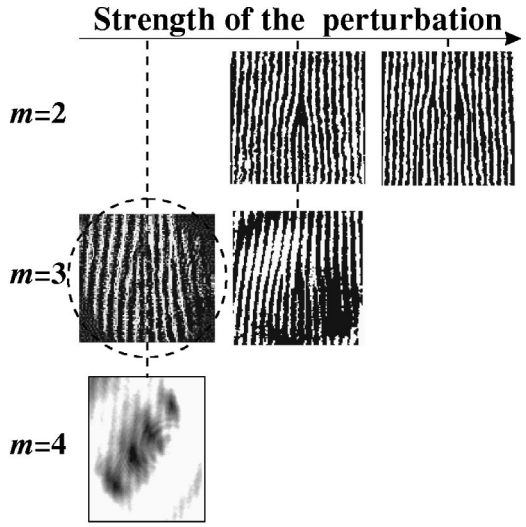

FIG. 1. Experimentally recorded decay stages for OV beams with different TCs. Dashed circle: partial decay of triple-charged OV beam at a perturbation causing complete decay of a charge-4 beam.

the relation $\Omega_{\text{crit}}|_m > \Omega^2 > \Omega_{\text{crit}}|_{m-1}$ is able to initiate a decay in the mentioned way. The interval of perturbation frequencies

$$\Delta\Omega^2_{\text{crit}} = \frac{[1/r - (k_0/n_0)U_0^2 f'(U_0^2)](2m+1)/r^2}{(k_0/2n_0)[1-f(U_0^2)]} \quad (2.13)$$

will be evaluated later for the particular experimental conditions under which partial decay of the triple charged OV beam is observed.

III. EXPERIMENTAL CONDITIONS

The OV beam is created by illuminating a photolithographically fabricated CGH of binary type (grating period of 20 μm) with an Ar^+-ion laser beam ($\lambda = 488$ nm). The diffraction efficiency at first order is 9%. The first-order background beam with the OV is focused on the entrance of the NLM [ethylene glycol dyed with DODCI (Lambdachrome) to reach an absorption coefficient of $\alpha = 0.107\ \text{cm}^{-1}$]. The NLM is aligned in the object arm of an interferometer, whereas the zero diffraction order beam (without phase singularity) passes through the reference arm (see Fig. 1 in [19]). The interference pattern is projected directly on a CCD array of a resolution of 13 μm.

The pictures shown in Fig. 1 are recorded at a nonlinear propagation path length of 6 cm, at $P = 72.5$ mW, and at the same (for the different TCs) offsets of the focusing lens with respect to its central alignment. The center of the m-fold charged OV beam can be easily recognized as the point where m neighboring interference lines converge into one. The coexistence of displaced phase dislocations with TCs $|m|=2$ and $|m|=1$ as a result of an intentionally caused decay of a triple-charged OV beam is clearly seen (the frame in the dashed circle in Fig. 1). A similar picture is recorded at equal but opposite misalignment of the focusing lens, which indicates reproducibility. In view of the theoretical model presented in the preceding section, these pictures can be explained by the saturation of the nonlinearity, which suppresses effectively the DSS instability. As a result, the perturbation can be critical for an OV beam with TC three remaining noncritical for single- and twofold charged OVSs. The further increase of the perturbation results in a complete decay into three single-charged OVSs. It is interesting to note (second column of frames in Fig. 1) that such a perturbation is still noncritical for OVSs of charge $|m|=2$. On the other side, for $|m|=4$ the OV beam decays and the cores of the individual single-charged dark beams appear well separated. The complete decay is observed at approximately the same perturbation that caused only a partial decay of triple-charged OV beam (Fig. 1, first column of frames).

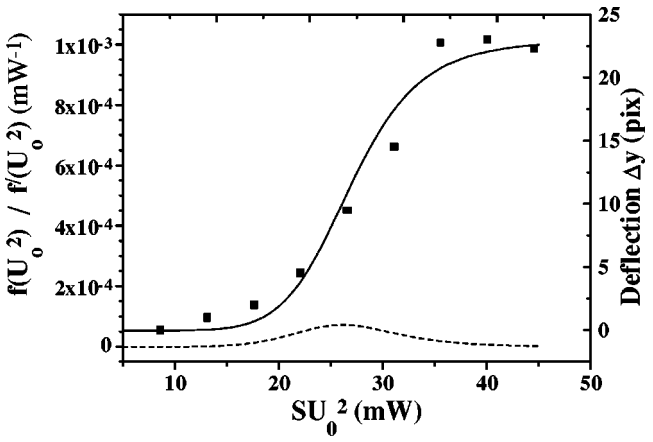

FIG. 2. Near-field self-deflection Δy of a half-cut Ar^+-laser beam after a nonlinear propagation path length of 10 cm (squares) and fit of the type $\Delta y \sim U_0^2/(1+U_0^2/U_{\text{sat}}^2)^3$ (solid curve). This fit is representative of the nonlinear contribution to the medium refractive index $f(U_0^2)$ [see Eqs. (2.2) and (2.3)] and for its first derivative $f'(U_0^2)$. (S-beam area at the entrance of the NLM.)

Another measurement is done in order to estimate quantitatively the saturation intensity $I_{\text{sat}} = (U_0^2)_{\text{sat}}$. The laser beam (without an OV nested in) is cut in half by a knife edge and is then imaged near the entrance window of the cell. The near-field beam deflection is measured by direct illumination of the CCD camera located 1.5 cm behind the 10 cm long NLM (Fig. 2, squares). The same scheme was used by Swartzlander and co-workers to study the self-bending effect in metal vapors [25] and in experiments on dark spatial soliton formation [26]. The best sigmoidal fit (solid line) yields a saturation power of $P_{\text{sat}} = S(U_0^2)_{\text{sat}} = 27(\pm 1)$ mW (S is the input beam cross section). This value is not sensitive to the particular saturation model. At the maximum self-deflection we estimate (see [25]) that the largest nonlinear correction to the refractive index of the medium reached is $\Delta n_{\max} = 10^{-3}$ ($\pm 15\%$). In the notations used in our theoretical analysis (see Sec. I) $f(U_0^2)$ is equal to Δn [Fig. 2, solid curve; see also Eqs. (2.2) and (2.3)]. The dashed curve in Fig. 2 presents the first derivative $f'(U_0^2)$, the values of which are necessary in evaluating the critical transverse spatial frequency Ω_{crit} [Eq. (2.12)]. The procedure described allows us to calculate the power/intensity dependence of Ω_{crit} for OVSs with different TCs (Fig. 3). It is worth noting the following.

(i) Since a single-charged OVS is generated at a power higher than $P_{\text{sat}} = (SU_0^2)_{\text{sat}}$ (denoted in Fig. 3 by a vertical

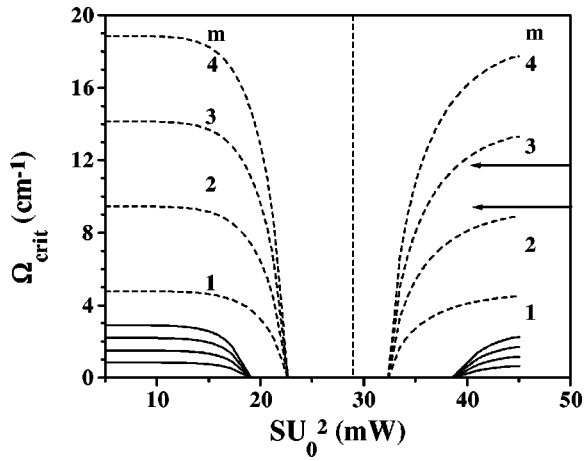

FIG. 3. Power dependence of the critical transverse spatial frequency of the perturbation for different TCs at radial offsets $1.0r_{OV}$ and $0.3r_{OV}$ (solid and dashed curves) from the vortex axis. Vertical dashed line is the saturation power measured (see Fig. 2). The arrows indicate the possible interval of perturbation frequencies for which the triple-charged OV beam decays [$\Omega<\Omega_{crit}$ $(m=3)$] into single- and double-charged OVSs [$(\Omega>\Omega_{crit}(m=1,2)$].

dashed line) and the soliton constant and background beam power increase with the TC [19], only the right-hand-side part of the curves in Fig. 3 should be considered in evaluating the OVS modulational stability. The left ones indicate the OV beam critical perturbation frequency in weakly and moderate nonlinear regimes.

(ii) The critical frequency Ω_{crit} is different for perturbations initiated at different radial coordinates r. The solid curves in Fig. 3 correspond to $r=r_{OV}$, the dashed ones to $r=0.3r_{OV}$. At a fixed input power it is seen that the critical frequency increases as the perturbation approaches the OV beam axis. It is easy to show [see Eq. (2.12)] that for perturbations arising at a distance shorter than $r_{crit}=[(k_0/n_0)U_0^2f'(U_0^2)]^{-1}$, Ω_{crit} is always a positive and fast growing function of the power/intensity above $(SU_0^2)_{sat}$. The OVSs are extremely sensitive to modulations. For our experimental conditions r_{crit} is 20 μm and equals the CGH grating period.

(iii) There exists an interval of transverse perturbation frequencies according to Eq. (2.13). The black arrows on the right side of Fig. 3 are intended to visualize this interval quantitatively for $|m|=3$ and a perturbation at $r=0.4r_{OV}$. Since a perturbation of frequency $\Omega<\Omega_{crit}$ $(m=3)$ starts to grow exponentially, the triple-charged dark beam decays. However, the critical frequencies Ω_{crit} $(m=1,2)$ are lower than Ω and an intermediate stabilization of the decay at OVSs with charges $|m_1|=1$ and $|m_2|=2$ is possible.

IV. NUMERICAL SIMULATIONS

The analysis presented in Sec. II is based on linearized equations for the evolution of radial perturbations to the amplitude and phase of the soliton. Generally, the perturbations can also depend on the azimuthal angle φ, i.e., $a=a(r,\varphi,z)$, $\Phi=\Phi(r,\varphi,z)$. Unfortunately, such an ansatz and the subsequent linearization result in partial differential equations for the perturbation amplitudes, which should be solved numerically [27,28]. The necessity to study later evolution stages of the vortices and the fact that each initial pure phase (or amplitude) perturbation develops inevitably both amplitude and phase modulation motivated us to carry out extended numerical simulations based on the GNLSE [Eq. (2.1)]. The latter is solved by a two-dimensional beam propagation method over 1024×1024 grid points. The background beam used is of a super-Gaussian form and has a full width at half maximum (FWHM) of r_{BG}, which is 45 times larger than that of a single-charged OVS. For a better visualization, the results presented below show some 0.55% of the total area of the computation window only. In the gray-scale phase images, white and black denote phases of 0 and 2π, respectively. The position of an OV beam is given by the point around which the phase increases monotonically from 0 to 2π.

A. One-dimensional perturbations

In our preceding numerical analyses [29], we observed that multiple-charged OVSs lose their identity and decay after collision with a ring dark solitary wave (RDSW). Because of its nonzero transverse velocity [30], at sufficiently large propagation distance this wave penetrates into the OVS core and initiates an unavoidable instability due to the $(1/r)$ dependence in the critical spatial perturbation frequency [Eq. (2.12); see also Fig. 3]. In order to keep the freedom of varying independently its initial position, period, and contrast, we preferred to start the simulations with the one-dimensional, initially pure amplitude modulation of the type

$$a(z=0)=a_0\cos\{k(x+\Delta)\},\qquad \Phi(z=0)=0, \tag{4.1}$$

where $2\pi/k\in[0.1,2]r_{BG}$. The results obtained confirmed that the modulational instability growth rate strongly depends on the position Δ, at which the perturbation is initiated, and decreases with increasing the saturation. In the rest of this section the data refer to a saturation parameter $s=I/I_{sat}=0.6$.

B. General form of the radial and azimuthal perturbation

In order to keep the correspondence between the present simulations and the theoretical model (Sec. II) as close as possible, the radial and azimuthal perturbations considered have the form

$$a(z=0)=a_0\exp(im\varphi)\exp\{i(Kr-N\varphi)\},\qquad \Phi(z=0)=\Phi_0\exp\{i(Kr-N\varphi)\}, \tag{4.2}$$

where K and the integer N denote the radial and azimuthal wave numbers of the perturbation, respectively. Before discussing the two particular cases of pure amplitude and pure phase perturbations, it is worth noting that neither of them remain ''pure'' at the later stages of the evolution.

Case 1. $K=0$, $N\neq0$ (initial azimuthal perturbation). In Fig. 4, we have plotted the number of the screw-type phase dislocations clearly identified at a nonlinear propagation distance $z=5L_{NL}$ as a function of the azimuthal wave number N. It was found that the instability of the m-fold charged OV beam is observed only in a finite region of values of N. For

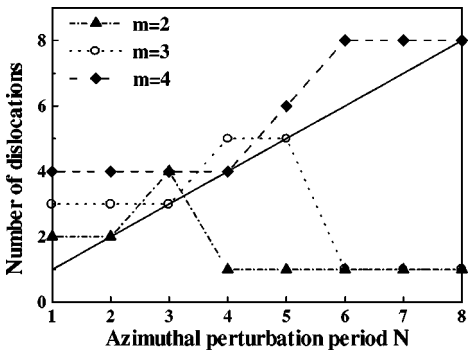

FIG. 4. Number of the screw phase dislocations distinguished at $z=5L_{\mathrm{NL}}$ vs azimuthal perturbation wave number N (solid line, $N=m$).

OVSs with TCs $m=2$ and 3, it terminates at $N=4$ and 6, respectively. No upper instability limit versus N was reached for the fourfold-charged OVSs at the highest azimuthal wave number of the perturbations $N_{\max}=8$ in the simulations (this limit is posed by the fidelity in recognizing clearly the screw phase dislocations at remaining highly overlapped OV-beam cores). The straight line $m=N$ in Fig. 4 is intended to accentuate on the three most important features: At azimuthal wave numbers N less than or equal to the TC m, the OVSs decay topologically into m vortices with unit circulations (Fig. 5, first row). At $N=m+1$, new pairs of phase dislocations are born (Fig. 5, second row). The higher the TC, the larger the number of the vortices created (see Fig. 4). This is a strong indication for the increase of the OVS modulational sensitivity at higher TCs. The transition from topological decay (and creation of new dislocations) to topological (meta)stability at increased N seems abrupt, thus indicating a maximum of the instability growth rate at $N>m+1$ (see Fig. 4).

Making use of the perturbation [Eqs. (4.2)] in its general form, with $m=3$, $N=1$ we observed the seemingly partial decay shown in Fig. 6. The conditions of this simulation correspond to a relatively low instability growth rate. In the absence of saturation of the nonlinearity, the decay was complete and substantially more strongly pronounced. The saturation (even when twice as high as the experimentally estimated value of $s=0.6$) was not able to cancel for the topological instability, but reduced it effectively. The initial perturbation of the background beam, however, corresponds to a (single) long-period azimuthal modulation forcing the OV beam to steer on the background [20,31]. Because of this, at $z=4L_{\mathrm{NL}}$ the phase dislocations with $m=1$ and $m=2$ are considerably offset from the center of the computation window. The same mechanism seems to complete later (at $z=10L_{\mathrm{NL}}$) the seemingly partial decay into three single-charged OV beams, two of them with still highly overlapping cores.

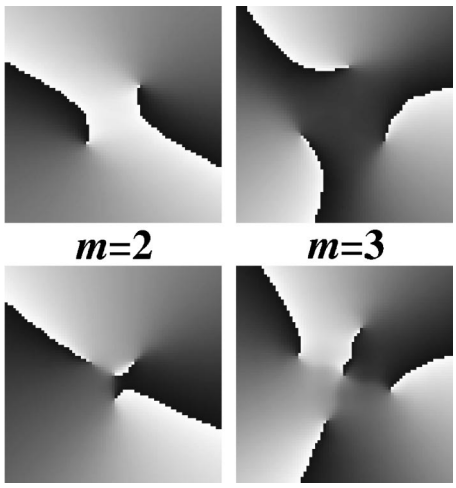

FIG. 5. Phase portraits of decayed OV beams with topological charges $m=2$ (left column) and 3 (right column) for azimuthal perturbation wave numbers $N=m$ (upper row) and $N=m+1$ (lower row).

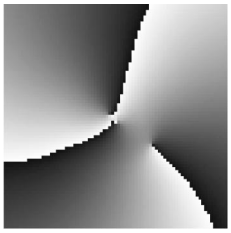

FIG. 6. Azimuthal perturbation: seemingly partial decay of an OV beam with TC $m=3$ into steering OV beam pair with TCs $m=2$ and $m=1$ $(z=4L_{\mathrm{NL}})$.

Case 2. $K\neq 0$, $N=0$ (radial perturbation). In this case the theoretical model given in Sec. II should be valid at the initial stage of the evolution of the perturbation. At the later stages, however, we observed an intriguing dynamics strongly influenced by the creation of coaxial RDSWs. Their repulsive mutual interaction [32], the gray initial conditions of their generation, and the saturation of the nonlinearity resulted in negative initial transverse velocities [30,33]. While decreasing their radii, their contrast increases and the radial phase variation at the RDSW becomes steeper [about 0.75π at $z=5L_{\mathrm{NL}}$; Fig. 7(b)]. The initially decayed and still highly overlapped single-charged OV beams [Fig. 7(a)] experience an increasing radial repulsion from the RDSW and partially recover the multiple-charged state [Fig. 7(b)]. This partial decay and recovering appears periodically in z (up to $z=10L_{\mathrm{NL}}$) with a period of approximately $2L_{\mathrm{NL}}$. The results presented in Fig. 7 are obtained at an initially pure amplitude radial perturbation of the type $[a(z=0)=a_0\exp(im\varphi)\cos(Kr),\ \Phi(z=0)=0]$. The perturbation in the general form given by Eq. (4.2) at $K\neq 0$ and $N=0$ corresponds to initial amplitude and phase radial modulations. Due to the substantially lower RDSW transverse velocity in this case we observed a decay, however the OV beam cores remained highly overlapped up to $10L_{\mathrm{NL}}$.

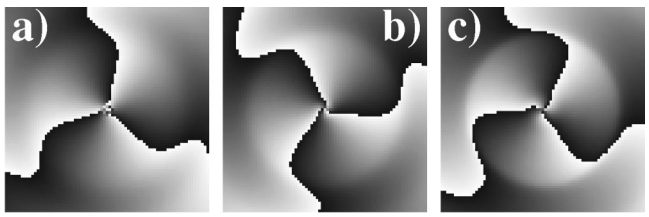

FIG. 7. Radial perturbation: Initial partial decay of a triple-charged OV beam (a) $(z=3L_{\mathrm{NL}})$ and subsequent recovering [(b) $z=5L_{\mathrm{NL}}$; (c) $z=9L_{\mathrm{NL}}$].

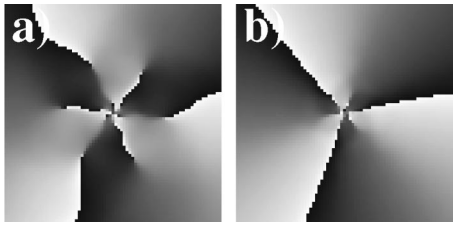

FIG. 8. Spiral perturbation: decay of triple-charged OV beam into 9 (a) and 3 (b) OV beams with overlapping cores at $z=5L_{\mathrm{NL}}$ and $2\pi/K=r_{\mathrm{BG}}/10$ and $2\pi/K=2r_{\mathrm{BG}}$, respectively.

Case 3. $K\neq 0$, $N\neq 0$ (spiral-type perturbation). In this case the perturbations have both radial and azimuthal components and show up as spirals starting from the OV-beam center. The results presented below refer to an OV beam with a topological charge $m=3$ and $N=6$, i.e., to a metastable, at an initial pure azimuthal perturbation (see Fig. 4), triple-charged OVS. However, the combined action of radial and azimuthal perturbations forces the dark beam to decay. At a radial perturbation period of $2\pi/K\approx r_{\mathrm{BG}}/5$, three new OV-beam pairs are born at $z=5L_{\mathrm{NL}}$ [Fig. 8(a)] and the total number of the dislocations becomes nine, while the total TC remains conserved [34]. The six identically charged OV beams form an outward lying hexagon and the three new oppositely charged phase dislocations remain offset, but still located near the beam axis. At $2\pi/K\approx 2r_{\mathrm{BG}}$ the strength of the instability is considerably lower, resulting in a decay into three single-charged OV beams [Fig. 8(b)]. No new pairs of phase dislocations are born.

The limiting case $2\pi/K\gg r_{\mathrm{BG}}$, i.e., at $K\rightarrow 0$, corresponds to a transition to the limit of azimuthal perturbations described in case 1. In the other limit of $2\pi/K\approx 0$ the radial perturbation period is very high and the perturbation approaches the radial one. The influence of the nonzero azimuthal wave number N, however, is not negligible. At $2\pi/K\approx r_{\mathrm{BG}}/10$ we observed at least 12 screw phase dislocations (almost the highest number, which is clearly identified within the discretization used).

V. CONCLUSION

We derived a general expression for the critical transverse spatial frequency Ω_{crit} for arbitrary charged OVSs imposed to a radial perturbation in a saturable local nonlinear media. The results confirm that saturation is able to suppress the modulational instability. If an instability is initiated, it can result in a partial decay of the highly charged OV beams. This concept is supported by experimental evidence. The measurement of the saturation intensity allowed an estimation of Ω_{crit} for the particular experimental conditions. The numerical simulations based on the GNLSE showed a rich variety of instability-evolution scenarios depending on the type of perturbation (azimuthal, radial, or mixed). The possibility to observe the partial decay as shown in Fig. 1 under saturation of the nonlinearity is confirmed for two different types of perturbations, both ensuring relatively low initial instability growth rates.

ACKNOWLEDGMENTS

A.D. would like to thank the Alexander von Humboldt Foundation for financial support and the opportunity to work in the stimulating atmosphere of the Max-Planck-Institut für Quantenoptik (Garching, Germany). This work was also supported by the Science Foundation of the Sofia University (Sofia, Bulgaria).

[1] Yu. S. Kivshar and B. Luther-Davies, Phys. Rep. **289**, 81 (1997), and references therein.
[2] G. P. Agrawal, *Nonlinear Fiber Optics* (Academic, Orlando, 1989).
[3] B. Luther-Davies, J. Christou, V. Tikhonenko, and Yu. S. Kivshar, J. Opt. Soc. Am. B **14**, 3046 (1997).
[4] N. B. Baravova, A. V. Mamaev, N. F. Pilipetsky, V. V. Shkunov, and B. Ya. Zel'dovich, J. Opt. Soc. Am. A **73**, 525 (1997).
[5] E. Abramochkin, N. Losevsky, and V. Volostnikov, Opt. Commun. **141**, 59 (1997).
[6] L. V. Kreminskaya, M. S. Soskin, and A. I. Khizhnyak, Opt. Commun. **145**, 377 (1998).
[7] N. R. Heckenberg, R. McDuff, C. P. Smith, and A. G. White, Opt. Lett. **17**, 221 (1992).
[8] V. Yu. Bazhenov, M. S. Soskin, and V. M. Vasnetsov, J. Mod. Opt. **39**, 985 (1992).
[9] M. W. Beijersbergen, R. C. P. Coerwinkel, M. Kristensen, and J. P. Woerdman, Opt. Commun. **112**, 3217 (1994).
[10] G. P. Brand, J. Mod. Opt. **45**, 215 (1998).
[11] G. A. Swartzlander,Jr., D. L. Drugan, N. Hallak, M. O. Freeman, and C. T. Law, Laser Phys. **5**, 704 (1995).
[12] A. Berzanskis, A. Matijous, A. Piskarskas, V. Smiglevicius, and A. Stabinis, Opt. Commun. **140**, 273 (1997).
[13] G. A. Swartzlander,Jr. and C. T. Law, Phys. Rev. Lett. **69**, 2503 (1992); see also G.-H. Kim, J.-H. Jeon, K.-H. Ko, H.-J. Moon, J.-H. Lee, and J.-S. Chang, Appl. Opt. **36**, 8614 (1997); G.-H. Kim, J.-H. Jeon, Y.-C. Noh, K.-W. Ko, H.-J. Moon, J.-H. Lee, and J.-S. Chang, Opt. Commun. **147**, 131 (1998).
[14] C. T. Law and G. A. Swartzlander, Jr., Opt. Lett. **18**, 586 (1993); V. Tikhonenko, J. Christou, B. Luther-Davies, and Yu. S. Kivshar, *ibid.* **21**, 1129 (1996).
[15] B. Luther-Davies, R. Powles, and V. Tikhonenko, Opt. Lett. **19**, 1816 (1994).
[16] I. V. Basistiy, V. Yu. Bazhenov, M. S. Soskin, and M. V. Vasnetsov, Opt. Commun. **103**, 422 (1993).
[17] A. V. Mamaev, M. Saffman, and A. A. Zozulya, Phys. Rev. Lett. **78**, 2108 (1997).
[18] J. C. Neu, Physica D **43**, 385 (1990); **43**, 407 (1990).
[19] A. Dreischuh, G. G. Paulus, F. Zacher, F. Grasbon, and H. Walther, Phys. Rev. E **60**, 6111 (1999).
[20] D. Rozas, C. T. Law, and G. A. Swartzlander, Jr., J. Opt. Soc. Am. B **14**, 3054 (1997).
[21] Z. Yovanovski and R. A. Sammut, Phys. Scr. **57**, 233 (1998).
[22] V. Tikhonenko, Yu. S. Kivshar, and V. V. Steblina, J. Opt. Soc. Am. B **15**, 79 (1998).
[23] Yu. S. Kivshar, D. Anderson, and M. Lisak, Phys. Scr. **47**, 679 (1993).

[24] D. Rozas, Z. S. Sacks, and G. A. Swartzlander, Jr., Phys. Rev. Lett. **79**, 3399 (1997) **[**Ref. [10] and the comment after Eq. (3)**]**.
[25] G. A. Swartzlander, Jr., H. Yin, and A. E. Kaplan, Opt. Lett. **13**, 1011 (1988).
[26] G. A. Swartzlander, Jr., D. R. Anderson, J. J. Regan, H. Yin, and A. E. Kaplan, Phys. Rev. Lett. **66**, 1583 (1991).
[27] W. J. Firth and D. V. Skryabin, Phys. Rev. Lett. **79**, 2450 (1997).
[28] G. Molina-Terriza, J. P. Torrez, L. Torner, and J. M. Soto-Crespo, Opt. Commun. **158**, 170 (1998).
[29] I. Velchev, A. Dreischuh, D. Neshev, and S. Dinev, Opt. Commun. **140**, 77 (1997).
[30] Yu. S. Kivshar and X. Yang, Phys. Rev. E **50**, R40 (1994).
[31] Yu. S. Kivshar, J. Christou, V. Tikhonenko, B. Luther-Davies, and L. Pismen, Opt. Commun. **152**, 198 (1998).
[32] V. Kamenov, A. Dreischuh, and S. Dinev, Phys. Scr. **55**, 68 (1997).
[33] W. Krolikowski, N. Akhmediev, and B. Luther-Davies, Phys. Rev. E **48**, 3980 (1993).
[34] I. Freund, Opt. Commun. **159**, 99 (1999).